crystals

MDPI

Article

Low-Frequency Band Gap Expansion of Acoustic Metamaterials Based on Multi-Mode Coupling Effect

Yudong Wu [1], Zhiyuan Wu [2], Wang Yan [1], Shiqi Deng [1], Fangjun Zuo [1], Mingliang Yang [2,*] and Weiping Ding [2]

[1] School of Intelligent Manufacturing, Chengdu Technological University, Chengdu 611730, China; ydwu@swjtu.edu.cn (Y.W.); shiqi_deng@yeah.net (S.D.); zuofangjun@126.com (F.Z.)
[2] School of Mechanical Engineering, Southwest Jiaotong University, Chengdu 610031, China
* Correspondence: yml@swjtu.edu.cn

Abstract

To address the problem of low-frequency broadband vibration and noise encountered in engineering, a method for expanding the low-frequency band gap of locally resonant acoustic metamaterials is proposed based on the multi-mode coupling effect. A computational method for the band gap characteristics of second-order multi-mode acoustic metamaterials has been derived. By incorporating the vibrational modes obtained from band structure calculations, a systematic investigation of the formation mechanisms of multiple band gaps was conducted, revealing that the emergence of these multiple band gaps stems from the coupled resonance between elastic waves and distinct vibrational modes of the local resonator units. Furthermore, the influence of design parameter variations on the bandgap was investigated, and the strategy of realizing low-frequency multi-order bandgaps by increasing the order of local resonance units was examined. Finally, vibration tests were conducted on the second-, third-, and fourth-order multi-mode coupled acoustic metamaterials. The results demonstrated that these materials exhibit an expanded vibration band gap within the low-frequency range, and the measured frequency response aligns closely with the theoretical calculations. This type of acoustic metamaterial offers viable applicability for controlling low-frequency broadband vibrations.

Keywords: acoustic metamaterials; multi-mode coupling; low-frequency; vibration reduction; band gap

check for updates

Academic Editor: Seiji Fukushima

Received: 8 August 2025
Revised: 22 August 2025
Accepted: 26 August 2025
Published: 27 August 2025

Citation: Wu, Y.; Wu, Z.; Yan, W.; Deng, S.; Zuo, F.; Yang, M.; Ding, W. Low-Frequency Band Gap Expansion of Acoustic Metamaterials Based on Multi-Mode Coupling Effect. *Crystals* **2025**, *15*, 764. https://doi.org/10.3390/cryst15090764

Copyright: © 2025 by the authors. Licensee MDPI, Basel, Switzerland. This article is an open access article distributed under the terms and conditions of the Creative Commons Attribution (CC BY) license (https://creativecommons.org/licenses/by/4.0/).

1. Introduction

Low-frequency vibrations and noise, characterized by their long propagation distances and strong penetration capabilities, have become significant challenges in both industrial and civilian sectors [1,2]. In industrial manufacturing, these low-frequency oscillations not only cause fatigue-related degradation and reduced precision of mechanical structures but also increase energy consumption and the risk of equipment failures. Similarly, in transportation, particularly automobiles, low-frequency noise inside the cabin significantly degrades the vehicle's Noise, Vibration, and Harshness (NVH) performance, potentially inducing adverse physiological effects in occupants [3–6].

In practical engineering applications, suppression of low-frequency vibration and noise predominantly depends on passive control methods, which fundamentally utilize the intrinsic properties of materials and structures to block or absorb vibrational energy. However, effective low-frequency sound insulation requires bulky and heavy structures,

rendering them impractical in space- and weight-constrained environments such as transportation vehicles and precision instruments [7–10]. Furthermore, due to the long wavelengths of low-frequency vibrations, conventional sound-absorbing materials and dampers demonstrate limited effectiveness in energy dissipation and fail to adequately address broadband low-frequency noise challenges [11,12]. Therefore, there is an urgent need to develop an innovative solution capable of mitigating broadband low-frequency vibration and noise.

The rapid advancement of acoustic metamaterials in recent years has introduced novel methods for controlling low-frequency vibrations and noise via subwavelength-scale structures. These configurations demonstrate significant elastic wave bandgaps and guided wave characteristics, making them highly promising for vibration attenuation and noise reduction applications. Thin-film and thin-plate structures are considered the most promising candidates for engineering implementation. After years of development, acoustic metamaterials have theoretically enabled lightweight control of low-frequency acoustic vibrations and have been experimentally validated, thereby enhancing their feasibility for practical engineering applications and broader adoption [13–18]. Based on the analogous propagation characteristics of sound waves in media to those of light waves, the concept of phononic crystals originated from photonic crystals [19,20]. Simultaneously, the study of acoustic wave transmission properties in phononic crystals has greatly benefited from insights into optical wave propagation phenomena in photonic crystals. According to Brillouin theory [21], when elastic waves propagate through periodically arranged units, distinct dispersion relations arise. Like photonic crystals, phononic crystals can modulate elastic (acoustic) waves within their structures through meticulous design and optimization of structural parameters. The concept of phononic crystals was first introduced by Kushwaha in 1993, utilizing the plane wave expansion method to elucidate the band characteristics along the shear direction of the structure [22]. Prior to 2000, research on phononic crystals primarily focused on their Bragg scattering properties. The ability of Bragg phononic crystals to manipulate elastic waves was strongly dependent on their structural thickness, often requiring the lattice dimensions to be on the same order of magnitude as the elastic wave wavelength to achieve effective wave control [23–25]. In 2000, Liu et al. introduced the concept of locally resonant phononic crystals, consisting of high-density lead spheres embedded in viscoelastic silicone rubber to form local resonance units [26]. Experimental analyses demonstrated that the elastic wave bandgap frequencies of these phononic crystals exceeded the limitations imposed by Bragg bandgaps, with lattice dimensions significantly smaller than the elastic wave wavelengths. The emergence of locally resonant phononic crystals therefore heralded the potential to manipulate long-wavelength waves using compact structures. Shen et al. developed a mathematical model for locally resonant phononic crystals, revealing that the effective mass density of the structure becomes negative as the phononic crystal approaches local resonance [27]. Wang et al., through detailed analysis of the vibrational characteristics and low-frequency bandgap properties of phononic crystals, proposed applying the lumped mass method to calculate the bandgap structures of locally resonant phononic crystals [28,29]. Some researchers have successfully controlled the bandgap width of phononic crystals by carefully adjusting their structural parameters [30–32]. Xiao et al. investigated the interaction between Bragg bandgaps and locally resonant bandgaps in rod or beam structures [33,34]. They analyzed the governing patterns of elastic wave bandgap properties and variations in local resonance frequencies, revealing the coexistence of two bandgap mechanisms within these structures. Through the coupling of these bandgaps, they achieved the formation of ultra-broad bandgaps.

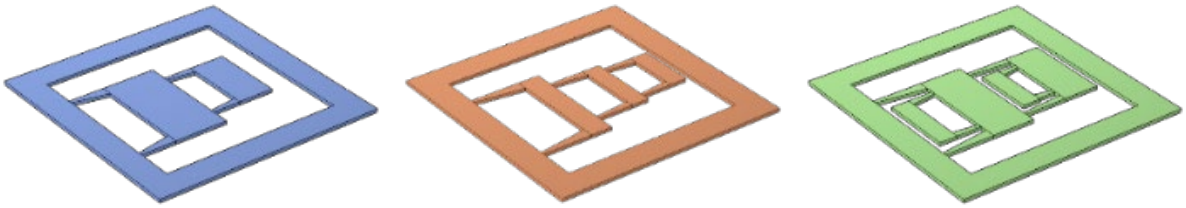
Acoustic metamaterials demonstrate exceptional low-frequency acoustic performance and, through careful design, have successfully addressed the challenge of singular low-

frequency peaks [35–37]. However, when tackling broadband low-frequency noise, acoustic metamaterials with single structural configurations fail to provide satisfactory results, highlighting the need to develop novel broadband noise attenuation acoustic metamaterials.

In this study, to address broadband low-frequency vibration and noise, a method predicated on multi-mode coupling effects has been proposed to expand the low-frequency bandgaps of locally resonant acoustic metamaterials. The rest of this paper is organized as follows. Section 2 presents the fundamental mechanism of bandgap formation in multi-mode coupling acoustic metamaterials. In Section 3, the influence of the design parameters and order increase on the bandgap is investigated. Section 4 shows the application in low-frequency vibration reduction with multi-mode acoustic metamaterials. Finally, the paper concludes with a summary presented in Section 5.

2. Formation of Band Gaps via Multi-Mode Coupling Effect

To investigate the bandgap characteristics of multi-mode acoustic metamaterials, a series of multi-mode cascaded locally resonant acoustic metamaterials plates were designed, as illustrated in Figure 1. Each locally resonant unit possesses a similar shape, albeit with different structural geometric dimensions.



(**a**) Two-order (**b**) Three-order (**c**) Four-order

Figure 1. Multi-mode acoustic metamaterials.

The finite element software COMSOL (version 6.2) was employed to model acoustic metamaterials and determine the band characteristics of infinitely periodic acoustic metamaterial plates, thereby elucidating the dispersion relationship between frequency and wave vector k. By analyzing the correlation between the band structure and characteristic modes, the formation mechanism of bandgaps in multi-mode acoustic metamaterials was revealed.

The governing equation describing the propagation of elastic waves in an isotropic, homogeneous medium is presented as Equation (1).

$$\rho\ddot{u} = \rho F + (\lambda + \mu)\nabla(\nabla \cdot u) + \mu\nabla^2 u \tag{1}$$

where u is displacement, F is the applied force, ρ is density, λ and μ are the Lamé constants and ∇ is the Nabla operator.

The proposed multi-mode coupled acoustic metamaterial model demonstrates infinite periodicity along the x–y plane.

According to the Bloch theorem, the bandgap calculation can be performed using a single unit cell [38]. Under the periodic boundary conditions of the original unit cell, the displacement must satisfy:

$$U(r,t) = e^{i(kr-\omega t)}U_k(r) \tag{2}$$

$$u(r+R) = U_k(r)e^{ikr} \tag{3}$$

where k is the Bloch wave vector confined within the first Brillouin zone, $U_k(r)$ is the amplitude modulation function, r is the lattice vector, ω is the angular frequency of the wave, R is the position vector and t is time.

Applying the periodic boundary conditions to the governing equation yields the characteristic equation:

$$\left(K - \omega^2 M\right) U = 0 \tag{4}$$

where K is the stiffness matrix of the cell, M is the mass matrix, U is the displacement matrix.

By traversing the wave vector (k) along the boundary of the irreducible Brillouin zone, one can obtain the band structure diagram; the irreducible Brillouin zone is depicted in Figure 2.

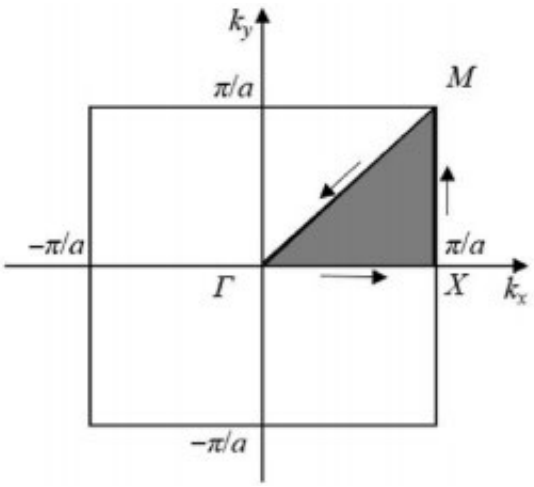


Figure 2. Irreducible Brillouin region.

To comprehensively examine the band characteristics of multi-mode coupled acoustic metamaterials, the two-order multi-mode acoustic metamaterial is selected as the computational model, with its structural parameters delineated in Figure 3.

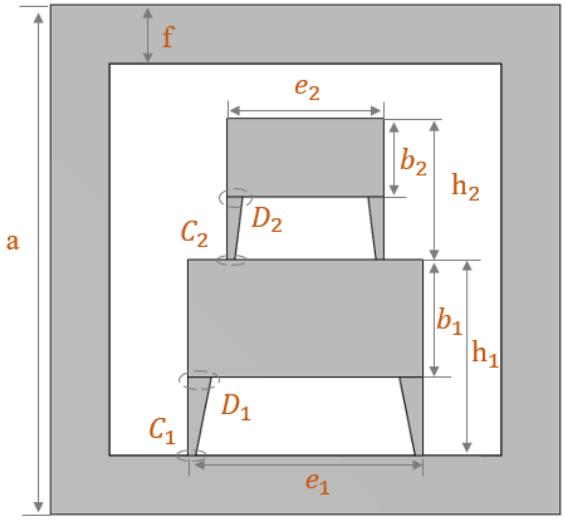


Figure 3. Structural parameters of two-order acoustic metamaterials.

Upon specifying the unit cell dimension (a) as 65 mm and the frame width (f) as 7.5 mm, the widths of the first-order cantilever beams (C_1) and (D_1) are 1 mm and 3 mm, respectively, the first-order resonator possesses a width (b_1) of 15 mm and a length (e_1) of 30 mm. Correspondingly, the widths of the second-order cantilever beams, (C_2) and (D_2), measure 1 mm and 2 mm respectively, while the second-order resonator exhibits a width

(b_2) of 10 mm and a length (e_2) of 20 mm, the band structure characteristics of the acoustic metamaterial can be determined. The band structure of the acoustic metamaterial was computed using COMSOL, with the results illustrated in Figure 4. As evident from the band diagram in Figure 4, the metamaterial exhibits two distinct band gaps under 800 Hz, spanning frequency ranges of 32.5–53.7 Hz and 212.8–289.8 Hz, respectively, resulting in a total band gap width of 98.2 Hz.

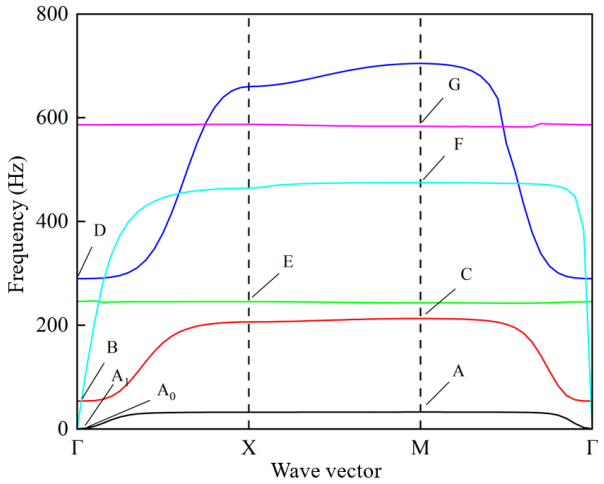


Figure 4. Band structure of two-order acoustic metamaterial.

Figure 4 distinctly reveals a series of nearly flat bands, including bands A and F along the X–M segment, as well as flat bands E and G, indicating that the structure possesses nearly identical intrinsic frequencies across different orientations. Each curve in the band diagram represents a specific vibration mode in the acoustic metamaterials, that is, the dispersion relationship of phonons. The vibration modes at the boundaries of each band gap are illustrated in Figure 5A,E–G demonstrate that the vibrational displacements are predominantly localized within the resonant units, while the displacements of the matrix framework remain negligible. Consequently, the vibrational energy is fully confined within the interior of the structure, characterizing these modes as quintessential localized resonance phenomena.

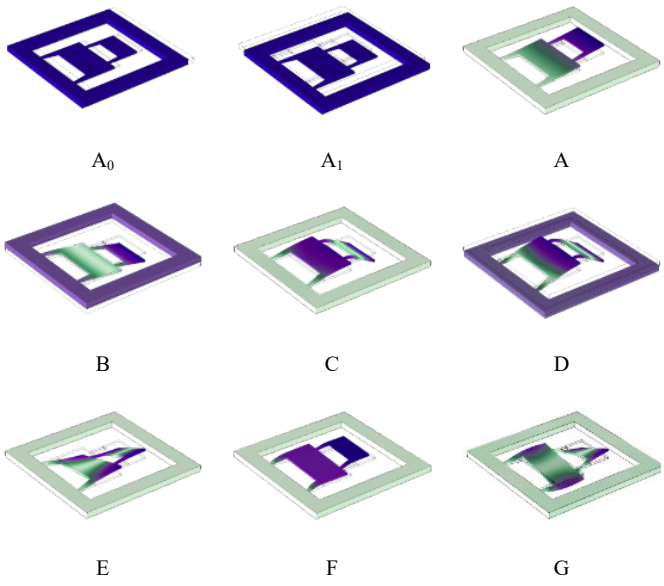


Figure 5. Local resonance modes of unit cell (**A_0–G** correspond to the different vibration modes for the band structure in Figure 4).

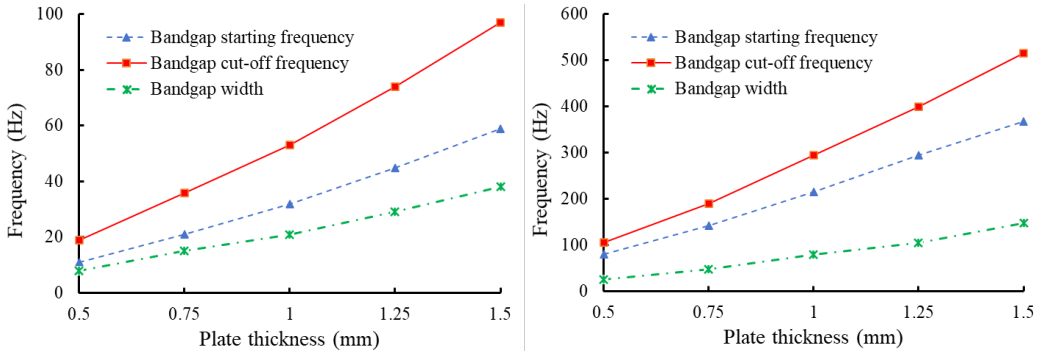
When the frequency of elastic waves propagating through the matrix framework approaches one of the natural frequencies of the resonant units, vibrations are transmitted from the matrix framework to the resonant units, thereby exciting the corresponding localized resonance modes. Simultaneously, the internal resonant units exert a reactive force on the matrix framework, coupling the elastic waves within the framework with this opposing force. Under such coupling, vibrations are suppressed. When the frequency of the elastic waves precisely matches the natural frequency of the resonant units, the reactive force generated by the resonators counterbalances the elastic wave excitation, thereby intensifying the coupling effect. As a result, the vibrations of the matrix framework are nearly completely neutralized by the reactive force, rendering it effectively immobile. Consequently, the resonant units obstruct the propagation of elastic waves within the matrix plate, giving rise to a band gap. As depicted in Figure 5A, the mode corresponding to the onset frequency of the first band gap reveals that displacement within the matrix framework is almost negligible. The resonant units are excited by the antisymmetric Lamb wave vibrating along the *z*-axis, causing them to oscillate in the same direction. The coupling between the resonant units and the antisymmetric Lamb wave thus opens the first bending wave band gap. The stronger the coupling, the wider the band gap; conversely, weaker coupling results in a narrower gap. Comparing the cutoff frequency mode at point B of the first band gap with the onset mode at point A, it is evident that, unlike the stationary matrix framework at mode A, the framework exhibits motion along the *z*-axis in mode B. Since the matrix framework is no longer static, the bending wave—specifically, the antisymmetric Lamb wave—can propagate through it unimpeded. Therefore, the first bending wave band gap terminates at point B. A similar analysis applies to the onset mode C and cutoff mode D of the second band gap. Modes E and G manifest as flat pass bands within the band structure diagram. These flat bands correspond to vibrational modes that traverse the entire Brillouin zone unimpeded and thus exert no influence on the formation or characteristics of the band gaps. Consequently, they lie outside the scope of the modes under consideration.

Therefore, the designed multi-mode coupled localized resonance acoustic metamaterial can induce resonances that generate band gaps in the low-frequency range. The width of these band gaps depends on the resonant units, the elastic wave modes in the plate, and the degree of their coupling. Stronger coupling of bending waves results in wider band gaps; conversely, weaker coupling leads to narrower band gaps.

3. Analysis of Influencing Factors and Order Increase

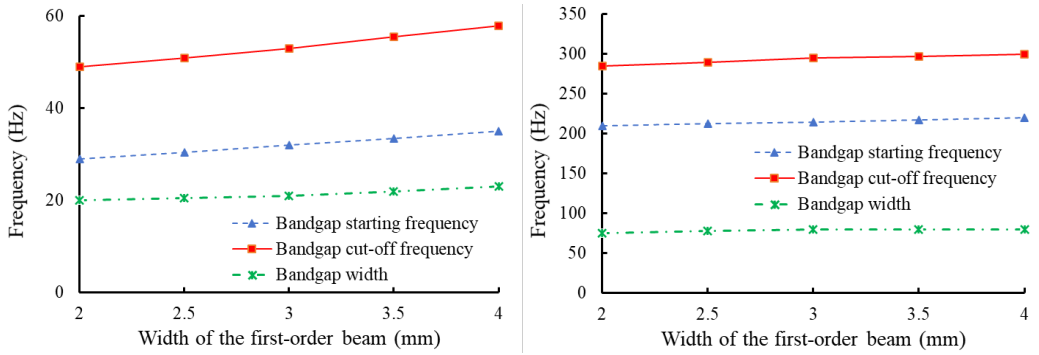
3.1. Analysis of Influencing Factors

To promote the application of multi-mode coupling acoustic metamaterials in low-frequency broadband vibration attenuation, the effect of unit cell structural design parameters on the band gap characteristics of the acoustic metamaterial plate is investigated. The structural parameters of the multi-mode acoustic metamaterial plate primarily include plate thickness, cantilever beam width and length, and oscillator mass. By adjusting these design parameters and applying them to band gap calculation formulas, the influence of parameter variations on the band gap characteristics of the multi-mode acoustic metamaterial plate is analyzed. By altering the structural parameters, band gaps were calculated, and their variations are illustrated in Figures 6–10.



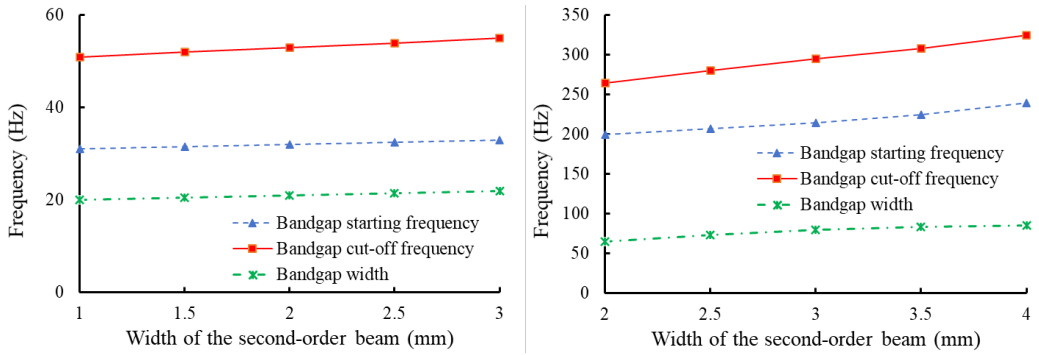
(**a**) The first band gap (**b**) The second band gap

Figure 6. Bandgap variation by changing the structure thickness.



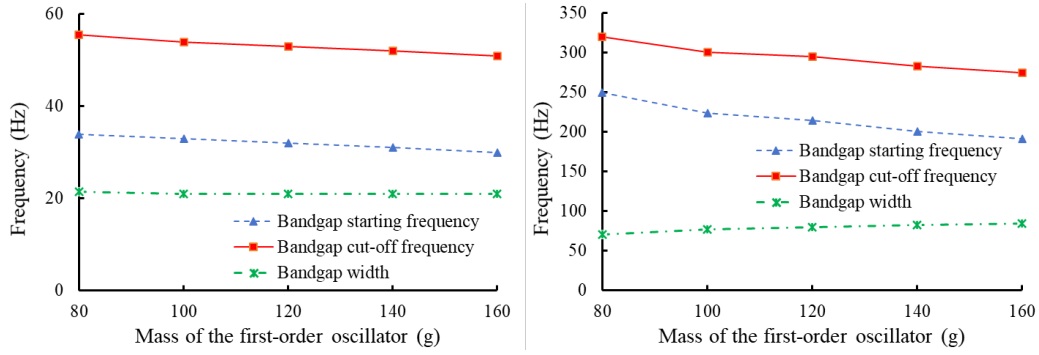
(**a**) The first band gap (**b**) The second band gap

Figure 7. Bandgap variation by changing the width of the first-order cantilever beam.



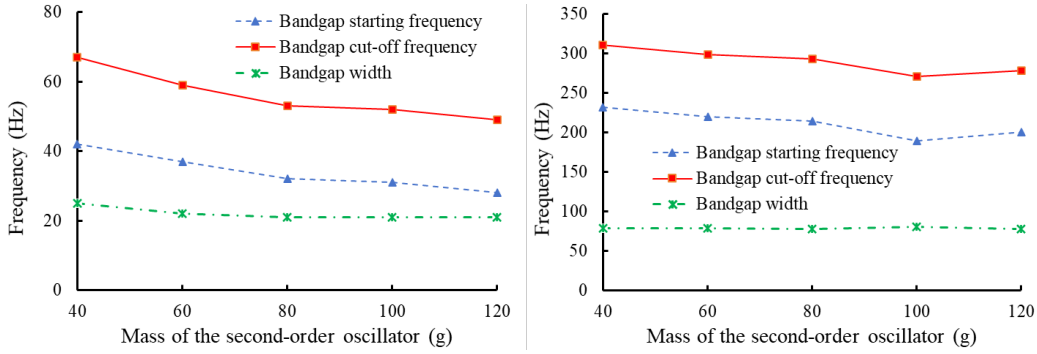
(**a**) The first band gap (**b**) The second band gap

Figure 8. Bandgap variation by changing the width of the second-order cantilever beam.



(**a**) The first band gap (**b**) The second band gap

Figure 9. Bandgap variation by changing the mass of the first-order oscillator.



(**a**) The first band gap (**b**) The second band gap

Figure 10. Bandgap variation by changing the mass of the second-order oscillator.

As shown in Figure 6, the band gaps are highly sensitive to changes in plate thickness. As the thickness increases, both the starting and cutoff frequencies of the first- and second-order band gaps shift to higher frequencies, with the cutoff frequencies being more sensitive to thickness variations. Consequently, the widths of these band gaps progressively increase, accompanied by an upward shift in their frequency ranges.

As illustrated in Figure 7, increasing the width of the first-order cantilever beam shifts both the starting and cutoff frequencies of the first-order band gap to higher frequencies, with the cutoff frequency being more sensitive to width changes, resulting in a slight increase in the band gap width. In contrast, the starting frequency, cutoff frequency, and position of the second-order band gap remain unchanged, with no variation in its width or location.

Figure 8 reveals that as the width of the second-order cantilever beam increases, the starting and cutoff frequencies of the first-order band gap remain nearly unchanged, with its width and position remaining relatively stable. In contrast, the starting and cutoff frequencies of the second-order band gap shift to higher frequencies, with the cutoff frequency more sensitive to width changes, causing a slight increase in the band gap width.

Figure 9 illustrates that as the first-order oscillator mass increases, both the starting and cutoff frequencies of the first-order band gap shift to lower frequencies, while its width remains unchanged. Similarly, the starting and cutoff frequencies of the second-order band gap also move to lower frequencies; however, the starting frequency is more sensitive to oscillator mass variations, resulting in an increased band gap width and a corresponding shift of the band gap position toward lower frequencies.

As illustrated in Figure 10, as the mass of the second-order oscillator increases, both the starting and cutoff frequencies of the first-order band gap shift to lower frequencies, accompanied by a decrease in band gap width. Similarly, the starting and cutoff frequencies of the second-order band gap also move to lower frequencies, while its band gap width remains unchanged.

3.2. Effects of Locally Resonant Unit Order Increase

Besides the geometric parameters of acoustic metamaterials, the order of locally resonant units in multi-mode coupling acoustic metamaterials also significantly affects their band gap characteristics. As the order increases, the coupled vibrations of the locally resonant units become more complex, and the types of vibration modes increase. Based on the structures shown in Figure 1b,c, their band structures are respectively calculated, as presented in Figures 11 and 12. Each curve in the band structure represents a specific vibration mode in the acoustic metamaterials and different band gaps are marked with areas of different colors.

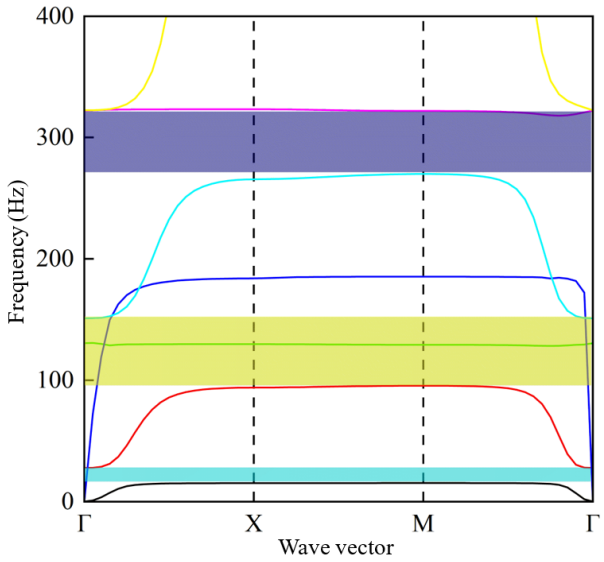


Figure 11. Band structure of three-order multi-mode acoustic metamaterial.

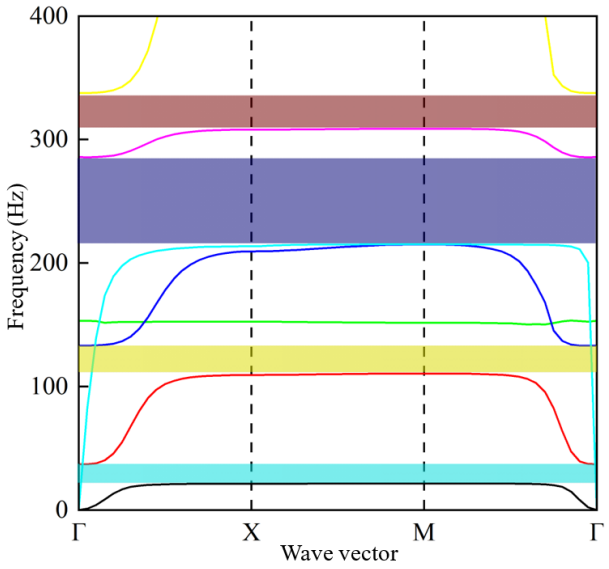


Figure 12. Band structure of four-order multi-mode acoustic metamaterial.

As illustrated in Figure 11, the three-order multi-mode acoustic metamaterial exhibits band gaps spanning 15.2–27.7 Hz, 98.5–151 Hz, and 270–322.5 Hz, with a total band gap width of 117.5 Hz. Figure 12 shows that the four-order multi-mode acoustic metamaterial has band gaps ranging from 21.5–37 Hz, 110.5–133.1 Hz, 215.2–285.8 Hz, and 308.8–337.7 Hz, with a total band gap width of 137.6 Hz. These results indicate that as the order of the multi-mode acoustic superstructure increases, both the number of band gaps and the total band gap width increase accordingly.

4. Validation of Vibration Reduction with Acoustic Metamaterials

To validate the low-frequency broadband vibration attenuation capabilities of the multi-mode coupling acoustic metamaterial, it was applied to a steel plate measuring 380 mm in length, 80 mm in width, and 1 mm in thickness. Vibration transfer function tests were conducted under excitation by an actuator. These tests involved two-order, three-order and four-order multi-mode coupling acoustic metamaterials, with the physical specimens shown in Figure 13.

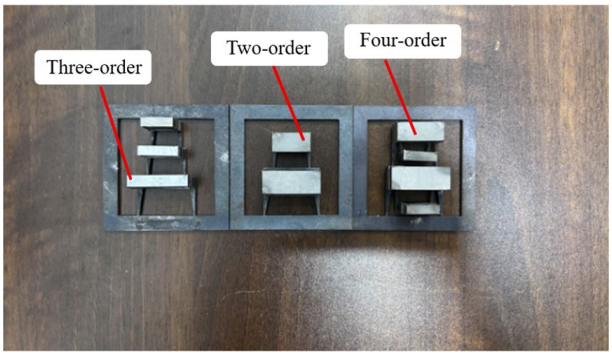


Figure 13. Experimental specimens of multi-mode acoustic metamaterials.

Five identical multi-mode coupling acoustic metamaterial unit cells were arranged on the steel plate structure. An actuator applied excitation perpendicular to the plate surface at one end, while an accelerometer was attached at the opposite end to measure vibration response signals normal to the plate surface. The plate was suspended by elastic cords to simulate free boundary conditions. The detailed experimental setup is shown in Figure 14.

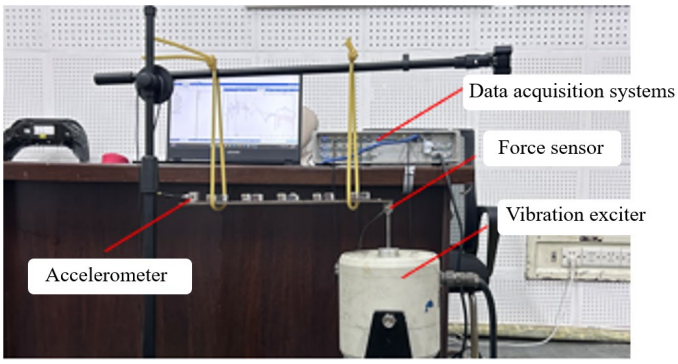


Figure 14. Experimental setup.

A broadband white noise signal ranging from 0 to 400 Hz was used to excite the steel plate through an actuator powered by a power amplifier. The force applied by the actuator was measured with a force sensor, while vibration acceleration at the plate's distal end was recorded by an accelerometer. Finally, the vibration frequency response function of the test specimen was calculated, as shown in Figures 15–17. The horizontal axis is the vibration frequency response function, and g is the unit of vibration acceleration, where $1g \approx 9.8\ m/s^2$.

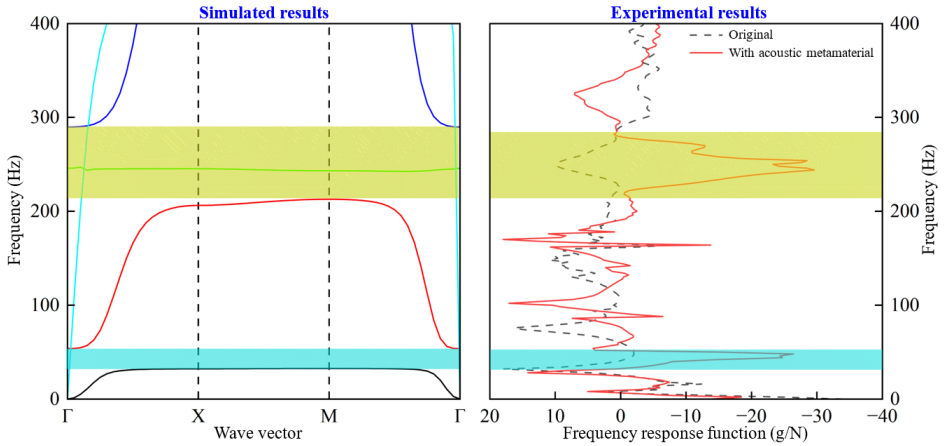


Figure 15. Comparison between simulated and experimental results of the two-order acoustic metamaterial.

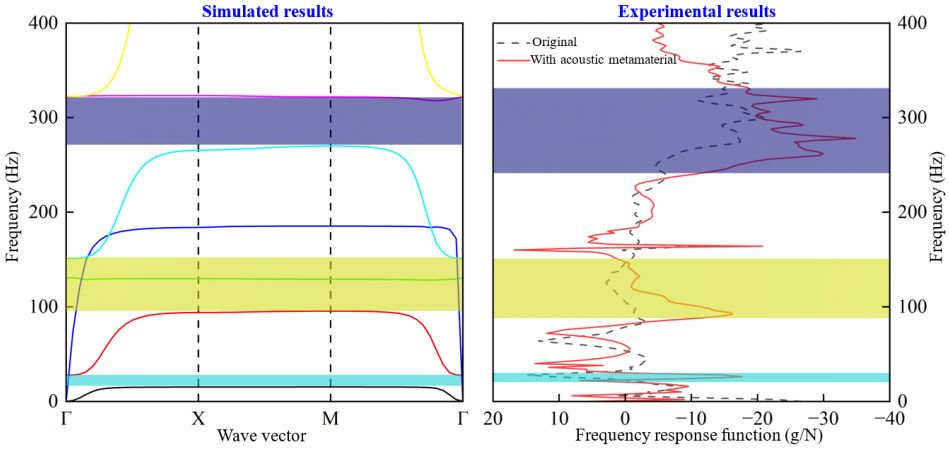


Figure 16. Comparison between simulated and experimental results of the three-order acoustic metamaterial.

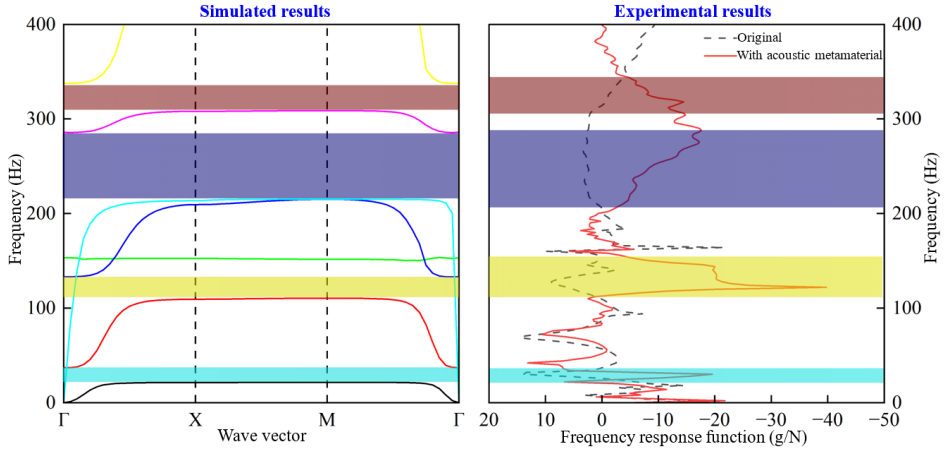


Figure 17. Comparison between simulated and experimental results of the four-order acoustic metamaterial.

It is illustrated in Figures 15–17 that, for the two-order, the three-order, and four-order multi-mode coupling acoustic metamaterials, the attenuation regions observed in experimentally measured vibration frequency response functions closely match the bandgap frequencies predicted by simulations. This effectively validates the presence of multiple low-frequency bandgaps in the multi-mode acoustic metamaterials, thereby achieving broadband vibration attenuation at low frequencies. Moreover, with increasing order of the locally resonant units, both the number of bandgaps and the overall bandgap width in the multi-mode coupling acoustic metamaterials increase correspondingly.

5. Conclusions

To address the challenge of low-frequency broadband vibration and noise in engineering applications, a multi-mode coupling acoustic metamaterial is proposed. This study elucidates the mechanism by which the coupling effects of multi-order locally resonant units extend the low-frequency bandgaps of acoustic metamaterials and experimentally validates the broadband low-frequency vibration attenuation characteristics of the multi-mode coupling acoustic metamaterial. The principal conclusions are as follows:

(1) The bandgaps of multi-mode coupling acoustic metamaterials are calculated using the finite element method. Analysis of various vibrational modes within the band structure reveals that the bandgap formation mechanism arises from the coupling

between the acoustic metamaterial and flexural waves in the substrate plate; notably, stronger coupling interactions lead to wider bandgaps.

(2) The influence of structural design parameters on the bandgaps of multi-mode coupling acoustic metamaterials was investigated. To achieve broader bandgaps, increasing the mass of the oscillators or enlarging the width of the cantilever beams can be considered; however, the latter tends to shift the bandgap toward higher frequencies. To promote the convergence of two bandgaps within the low-frequency domain, it is necessary to reduce the width of either the first- or second-order cantilever beams or, alternatively, increase the mass of the first- or second-order oscillators.

(3) As the order of the multi-mode acoustic superstructure increases, both the number of band gaps and the total band gap width increase accordingly.

(4) The attenuation regions observed in experimentally measured vibration frequency response functions closely match the bandgap frequencies predicted by simulations. This effectively validates the presence of multiple low-frequency bandgaps in the multi-mode acoustic metamaterials, thereby achieving broadband vibration attenuation at low frequencies.

In this study, the multi-mode coupling effect is utilized to increase both the number and total width of band gaps in acoustic metamaterials. This approach offers potential solutions to low-frequency vibration and noise problems encountered in engineering applications, such as low-frequency NVH (Noise, Vibration, and Harshness) issues in automobiles, which often consist of multiple dominant frequency bands. By carefully designing multi-mode coupling acoustic metamaterials, effective control of low-frequency vibrations and noise across multiple frequency bands can be achieved. However, achieving a continuous low-frequency broadband bandgap remains challenging, particularly under constraints on structural weight, and thus warrants further investigation.

Author Contributions: Methodology, Y.W.; software, S.D.; validation, Z.W. and W.Y.; project administration, F.Z.; funding acquisition, M.Y. and W.D. All authors have read and agreed to the published version of the manuscript.

Funding: This study was funded by the Science and Technology Program of Yibin [grant number 2024JC017], the Talent Program (Ph.D. Fund) of Chengdu Technological University [grant number 2024RC025], the Key Project of Chengdu Technological University [grant number 2025ZR004], the Natural Science Foundation of Sichuan Province [grant number 24NSFSC1295] and Fundamental Research Funds for the Central Universities [grant number XJ2021KJZK054].

Data Availability Statement: The data used to support the findings of this study are available from the corresponding author upon request.

Acknowledgments: The authors thank the China Automotive Technology & Research Center for supporting the completion of this work.

Conflicts of Interest: The authors declare that there are no conflicts of interest regarding the publication of this paper.

References

1. Broner, N. The effects of low frequency noise on people—A review. *J. Sound Vib.* **1978**, *58*, 483–500. [CrossRef]
2. Araújo Alves, J.; Neto Paiva, F.; Torres Silva, L.; Remoaldo, P. Low-frequency noise and its main effects on human health—A review of the literature between 2016 and 2019. *Appl. Sci.* **2020**, *10*, 5205. [CrossRef]
3. Panda, K.C. Dealing with noise and vibration in automotive industry. *Procedia Eng.* **2016**, *144*, 1167–1174. [CrossRef]
4. Iwabuki, H.; Fukada, S.; Osafune, T.; Shimura, M.; Sasaki, E. Contribution of large-vehicle vibration and bridge vibration to low-frequency noise generation characteristics. *Appl. Acoust.* **2019**, *155*, 150–166. [CrossRef]
5. Hazra, S.; Reddy, J.K. A review paper on recent research of noise and vibration in electric vehicle powertrain mounting system. *SAE Int. J. Veh. Dyn. Stab. NVH* **2021**, *6*, 3–22. [CrossRef]

6. Liao, Y.; Huang, H.; Chang, G.; Luo, D.; Xu, C.; Wu, Y.; Tang, J. Research on low-frequency noise control of automobiles based on acoustic metamaterial. *Materials* **2022**, *15*, 3261. [CrossRef]
7. Hodgdon, K.K.; Atchley, A.A.; Bernhard, R.J. *Low Frequency Noise Study*; Partnership for Air Transportation Noise and Emissions Reduction: Cambridge, MA, USA, 2007.
8. Zhao, Y.; Wang, X. A review of low-frequency active vibration control of seat suspension systems. *Appl. Sci.* **2019**, *9*, 3326. [CrossRef]
9. Ye, S.; Hou, L.; Zhang, P.; Bu, X.; Xiang, J.; Tang, H.; Lin, J. Transfer path analysis and its application in low-frequency vibration reduction of steering wheel of a passenger vehicle. *Appl. Acoust.* **2020**, *157*, 107021. [CrossRef]
10. Chen, D.; Li, Y.; Gong, Y.; Li, X.; Ouyang, W.; Li, X. Low frequency vibration isolation characteristics and intelligent design method of hull grillage metastructures. *Mar. Struct.* **2024**, *94*, 103572. [CrossRef]
11. Yang, M.; Chen, S.; Fu, C.; Sheng, P. Optimal sound-absorbing structures. *Mater. Horiz.* **2017**, *4*, 673–680. [CrossRef]
12. Huang, S.; Li, Y.; Zhu, J.; Tsai, D.P. Sound-absorbing materials. *Phys. Rev. Appl.* **2023**, *20*, 010501. [CrossRef]
13. Mei, J.; Ma, G.; Yang, M.; Yang, Z.; Wen, W.; Sheng, P. Dark acoustic metamaterials as super absorbers for low-frequency sound. *Nat. Commun.* **2012**, *3*, 756. [CrossRef]
14. Slagle, A.C.; Fuller, C.R. Low frequency noise reduction using poro-elastic acoustic metamaterials. In Proceedings of the 21st AIAA/CEAS Aeroacoustics Conference, Dallas, TX, USA; 2015; p. 3113.
15. Lee, S.; Ahn, C.H.; Lee, J.W. Vibro-acoustic metamaterial for longitudinal vibration suppression in a low frequency range. *Int. J. Mech. Sci.* **2018**, *144*, 223–234. [CrossRef]
16. Ning, S.; Yang, F.; Luo, C.; Liu, Z.; Zhuang, Z. Low-frequency tunable locally resonant band gaps in acoustic metamaterials through large deformation. *Extrem. Mech. Lett.* **2020**, *35*, 100623. [CrossRef]
17. Gao, N.; Zhang, Z.; Deng, J.; Guo, X.; Cheng, B.; Hou, H. Acoustic metamaterials for noise reduction: A review. *Adv. Mater. Technol.* **2022**, *7*, 2100698. [CrossRef]
18. Wu, L.; Zhai, Z.; Zhao, X.; Tian, X.; Li, D.; Wang, Q.; Jiang, H. Modular design for acoustic metamaterials: Low-frequency noise attenuation. *Adv. Funct. Mater.* **2022**, *32*, 2105712. [CrossRef]
19. Khelif, A.; Adibi, A. *Phononic Crystals*; Springer: Berlin/Heidelberg, Germany, 2015; Volume 10, ISBN 978-1461493921.
20. Lu, M.-H.; Feng, L.; Chen, Y.-F. Phononic crystals and acoustic metamaterials. *Mater. Today* **2009**, *12*, 34–42. [CrossRef]
21. Bouckaert, L.P.; Smoluchowski, R.; Wigner, E. Theory of Brillouin zones and symmetry properties of wave functions in crystals. *Phys. Rev.* **1936**, *50*, 58. [CrossRef]
22. Kushwaha, M.S.; Halevi, P.; Dobrzynski, L.; Djafari-Rouhani, B. Acoustic band structure of periodic elastic composites. *Phys. Rev. Lett.* **1993**, *71*, 2022. [CrossRef]
23. Vasseur, J.O.; Deymier, P.; Frantziskonis, G.; Hong, G.; Djafari-Rouhani, B.; Dobrzynski, L. Experimental evidence for the existence of absolute acoustic band gaps in two-dimensional periodic composite media. *J. Phys. Condens. Matter* **1998**, *10*, 6051. [CrossRef]
24. Lu, Y.-q.; Zhu, Y.-y.; Chen, Y.-f.; Zhu, S.-n.; Ming, N.-b.; Feng, Y.-J. Optical properties of an ionic-type phononic crystal. *Science* **1999**, *284*, 1822–1824. [CrossRef] [PubMed]
25. Tanaka, Y.; Tamura, S.-i. Acoustic stop bands of surface and bulk modes in two-dimensional phononic lattices consisting of aluminum and a polymer. *Phys. Rev. B* **1999**, *60*, 13294. [CrossRef]
26. Liu, Z.; Zhang, X.; Mao, Y.; Zhu, Y.Y.; Yang, Z.; Chan, C.T.; Sheng, P. Locally resonant sonic materials. *Science* **2000**, *289*, 1734–1736. [CrossRef] [PubMed]
27. Page, J.; Sukhovich, A.; Yang, S.; Cowan, M.; Van Der Biest, F.; Tourin, A.; Fink, M.; Liu, Z.; Chan, C.; Sheng, P. Phononic crystals. *Phys. Status Solidi (B)* **2004**, *241*, 3454–3462. [CrossRef]
28. Wang, G.; Wen, X.; Wen, J.; Shao, L.; Liu, Y. Two-dimensional locally resonant phononic crystals with binary structures. *Phys. Rev. Lett.* **2004**, *93*, 154302. [CrossRef]
29. Wang, G.; Wan, S.; Hong, J.; Liu, S.; Li, X. Analysis of flexural and torsional vibration band gaps in phononic crystal beam. *J. Vib. Control* **2023**, *29*, 4814–4827. [CrossRef]
30. Khelif, A.; Aoubiza, B.; Mohammadi, S.; Adibi, A.; Laude, V. Complete band gaps in two-dimensional phononic crystal slabs. *Phys. Rev. E—Stat. Nonlinear Soft Matter Phys.* **2006**, *74*, 046610. [CrossRef]
31. Wu, Y.; Yan, W.; Wen, G.; He, Y.; Deng, S.; Ding, W. Design and Application of a Lightweight Plate-Type Acoustic Metamaterial for Vehicle Interior Low-Frequency Noise Reduction. *Crystals* **2024**, *14*, 957. [CrossRef]
32. D'Alessandro, L.; Belloni, E.; Ardito, R.; Corigliano, A.; Braghin, F. Modeling and experimental verification of an ultra-wide bandgap in 3D phononic crystal. *Appl. Phys. Lett.* **2016**, *109*, 221907. [CrossRef]
33. Xiao, Y.; Wen, J. Closed-form formulas for bandgap estimation and design of metastructures undergoing longitudinal or torsional vibration. *J. Sound Vib.* **2020**, *485*, 115578. [CrossRef]
34. Xiao, Y.; Wen, J.; Wen, X. Broadband locally resonant beams containing multiple periodic arrays of attached resonators. *Phys. Lett. A* **2012**, *376*, 1384–1390. [CrossRef]

35. Deng, S.; He, Y.; Wu, Y.; Ding, W. A locally resonant metamaterial beam with tunable electromagnetic stiffness based on the electromechanical analogy network. *Smart Mater. Struct.* **2024**, *33*, 055052. [CrossRef]
36. Krushynska, A.; Bosia, F.; Miniaci, M.; Pugno, N. Spider web-structured labyrinthine acoustic metamaterials for low-frequency sound control. *New J. Phys.* **2017**, *19*, 105001. [CrossRef]
37. Gao, N.; Lu, K. An underwater metamaterial for broadband acoustic absorption at low frequency. *Appl. Acoust.* **2020**, *169*, 107500. [CrossRef]
38. Laude, V.; Achaoui, Y.; Benchabane, S.; Khelif, A. Evanescent Bloch waves and the complex band structure of phononic crystals. *Phys. Rev. B—Condens. Matter Mater. Phys.* **2009**, *80*, 092301. [CrossRef]

Disclaimer/Publisher's Note: The statements, opinions and data contained in all publications are solely those of the individual author(s) and contributor(s) and not of MDPI and/or the editor(s). MDPI and/or the editor(s) disclaim responsibility for any injury to people or property resulting from any ideas, methods, instructions or products referred to in the content.